Article

DNA Motion Capture Reveals the Mechanical Properties of DNA at the Mesoscale

Allen C. Price,[1] Kevin R. Pilkiewicz,[2] Thomas G. W. Graham,[3,4] Dan Song,[4,5] Joel D. Eaves,[2,*] and Joseph J. Loparo[4,*]

[1]Department of Chemistry and Physics, Emmanuel College, Boston, Massachusetts; [2]Department of Chemistry and Biochemistry, University of Colorado, Boulder, Colorado; [3]Department of Systems Biology, [4]Department of Biological Chemistry and Molecular Pharmacology, and [5]Harvard Biophysics Program, Harvard Medical School, Boston, Massachusetts

ABSTRACT Single-molecule studies probing the end-to-end extension of long DNAs have established that the mechanical properties of DNA are well described by a wormlike chain force law, a polymer model where persistence length is the only adjustable parameter. We present a DNA motion-capture technique in which DNA molecules are labeled with fluorescent quantum dots at specific sites along the DNA contour and their positions are imaged. Tracking these positions in time allows us to characterize how segments within a long DNA are extended by flow and how fluctuations within the molecule are correlated. Utilizing a linear response theory of small fluctuations, we extract elastic forces for the different, ~2-μm-long segments along the DNA backbone. We find that the average force-extension behavior of the segments can be well described by a wormlike chain force law with an anomalously small persistence length.

INTRODUCTION

The mechanical properties of DNA play crucial roles in biological transactions and in nanoscale devices (1–3). Negative charges along the backbone, basepair stacking, and intrastrand hydrogen bonding make DNA rigid on small length scales, whereas on length scales much greater than that of a covalent bond, the polymer behaves like a semiflexible elastic object (4). Some of the first single-molecule force-pulling experiments showed that on these length scales, DNA can be described using the wormlike chain (WLC) model (4–6). In the WLC model, the polymer is treated as an inextensible rod with a finite bending rigidity. In its most common form, this model has one parameter, the persistence length, which characterizes the typical radius of curvature at thermal equilibrium. The persistence length of DNA in solution is ~150 basepairs, or 50 nm. Although the WLC model is successful at describing the conformations of DNA in solution, in vivo DNAs are often subjected to bending radii much smaller than the equilibrium persistence length (7). For example, the linear dimensions of chromosomes are orders of magnitude smaller than the DNA contour length due to several levels of compaction. Genomic DNA is wrapped around 10 nm nucleosomes and then packaged further through the formation of trapped DNA loops and other domains. DNA binding proteins facilitate and stabilize the formation of these trapped DNA loops, modulating the mechanical properties of DNA on length scales much longer than that of their binding sites (8,9). The elastic properties of DNA on the mesoscale, which includes length scales larger than a few basepairs but smaller than the total polymer length, are thus biologically important, but they are also poorly understood.

Previous single-molecule studies on the mechanical properties of DNA have employed optical tweezers, magnetic beads, electric fields, and flows to measure the stretching response of individual DNA molecules (10,11). With few exceptions, these studies have focused on how the total end-to-end extension varies with the applied force. This gives a measure of the reversible work necessary to increase the end-to-end distance of the polymer, which is effectively a measure of the polymer's Helmholtz free energy. Statistical mechanics and the central limit theorem guarantee that for a sufficiently long polymer, this energy will be independent of the specific nature of the interactions between individual segments of the molecule. Hence, these experiments are not capable of probing mesoscale dynamics. By the same token, theoretical models that treat the polymer as effectively uniform over its contour length, such as the Rouse (12,13), Zimm (14), and even the WLC model, although suitable for describing the large-scale end-to-end dynamics of polymer chains, may be inadequate at describing DNA on the mesoscale. Indeed, recent single-molecule experiments on short DNA strands (15–17) have shown marked deviations from the predictions made by the WLC model, although it is not clear how the end-to-end forces experienced by these submicron pieces of DNA are related to those experienced by polymer segments

Submitted November 5, 2014, and accepted for publication April 20, 2015.

*Correspondence: joseph_loparo@hms.harvard.edu or joel.eaves@colorado.edu

Editor: David Rueda.

0006-3495/15/05/2532/9 $2.00

http://dx.doi.org/10.1016/j.bpj.2015.04.022

measuring on the order of a micron inside a several-micron-long DNA molecule.

In this article, we address this current gap in the picture of DNA by using, to our knowledge, a novel single-molecule microscopy approach in concert with theory. Inspired by motion-capture technology used in high-speed photography and computer animation, we examine the dynamics of DNA by site-specifically labeling the polymer with fluorescent reporters and dynamically tracking the motion of individual links of the DNA chain as they move under flow in real time. The time-averaged extension of the individual links shows the nonuniform stretching of a surface-tethered DNA in shear flow. In addition, calculations of correlations of the fluctuations in both the transverse and in-flow directions show highly correlated motions as well as equivalent time scales of fluctuations at all points along the DNA. These observations are consistent with a single mode dominating the fluctuations.

We analyze the covariance matrix of the fluctuations using a theory for small-amplitude fluctuations of linear polymer segments (18). This allows us to extract in a model-independent way the nonlinear force laws that describe the effective interactions between different points along the DNA chain and make quantitative measurements of the tension in different segments of the molecule. These quantities, which were previously inaccessible to experimental measurement, allow us to test the WLC model, originally developed for end-to-end extension, as it applies to segments within the DNA. We show that the model is consistent with our data, but only with a persistence length smaller than that reported by other studies.

MATERIALS AND METHODS

Protein preparations

*Eco*RI protein was purified as described in Graham et al. (38).

Single-molecule experiments

The functionalization of glass coverslips and the preparation and labeling of biotinylated λ DNA with quantum dots were carried out as described in Graham et al. (38). A flow cell with a linear channel 4 mm wide and 120 μm high was used. The surface of the flow cell was coated with streptavidin, washed, and incubated with preincubated *Eco*RI-E111Q-QD-labeled λ DNA for ~10 min or until tethers could be clearly seen. During data collection, the flow cell was washed with the low or high viscosity buffer (10 mM Tris, pH 8.0, 50 mM NaCl, 200 μg/mL BSA, 0.005% (v/v) Tween-20, 50% (w/w) sucrose was added for the high-viscosity buffer).

Motion capture technique

QDs were imaged with a home-built through-objective total internal reflection fluorescence microscope using 488 nm excitation (Sapphire 488-50, Coherent, Santa Clara, CA). Details of the microscope and its alignment can be found in Graham et al. (38). In flow stretching data collection protocols, only DNAs showing five quantum dots were collected. We eliminated DNAs that had nonspecifically bound QDs by aligning images of labeled DNAs at their tether points and only accepting DNAs that were full-length and showed QDs at consensus locations; nonspecifically bound QDs bound randomly to the DNA. DNAs with five QDs in the consensus locations represented ~10% of the total number of labeled DNAs. QDs typically remained bound to DNA for many minutes, although increasing flow rates increased the off rate. See Fig. S1 for a montage of a DNA fluctuating in flow.

Two types of flow stretching data were collected. To measure the static, time-averaged conformation of the DNA, at least 200 images were collected at a frame rate of 2 frames/s (fps) for each flow rate in the low-viscosity buffer. For the dynamic data, DNAs were imaged at either 88 fps or 32 fps for the low- or high-viscosity buffer, respectively. At least 10,000 frames were collected at each flow rate for each DNA molecule. To avoid bias introduced by overlap in the flow stretching data, the positions of all five QDs were determined in a single multiparameter fit. Tracking of single QDs nonspecifically stuck to the coverslip surface demonstrated that the fitted x and y positions varied by only 5–10 nm per frame, similar to the reported reproducibility in other single-particle experiments (22).

RESULTS

Visualizing DNA conformations with site-specific DNA labeling

Site-specific labeling of DNAs allows us to follow the position fluctuations of specific loci to better reconstruct DNA motion. Fig. 1 *a* provides an overview of our experimental approach. Genomic DNAs from bacteriophage λ were tethered to a PEG-passivated coverslip through biotin-streptavidin interactions. DNAs were labeled with a catalytically inactive mutant of the restriction endonuclease *Eco*RI–E111Q coupled to anti-His QDs (19,20). *Eco*RI–E111Q binds with high specificity to five endogenous sites within the λ genome (21226, 26104, 31747, 39168, and 44972 bp from the tether point) but is unable to cleave the DNA backbone and thus remains stably associated with the DNA. Laminar flow through the microfluidic flow cell acted to hydrodynamically stretch the DNAs. A home-built through-objective total internal reflection fluorescence microscope was used to follow DNA motion by imaging the DNA-associated QDs. Position trajectories of QDs were then harvested from the resulting movies by fitting two-dimensional Gaussian functions to the diffraction-limited images.

The total fractional extension of a polymer under shear flow depends exclusively upon the Weissenberg number (Wi) (23,24), a dimensionless number equal to the product of the rate of shear and the longest relaxation time of the polymer. We independently controlled both shear rate and relaxation rate of the DNA by varying the viscosity and flow rate of the solution. We collected data using both a low-viscosity buffer (viscosity ~1 cP) and a high-viscosity (50% sucrose) buffer. The viscosity of the latter buffer was calculated to be 15 cP based on the concentration of sucrose. The longest relaxation time, τ_0, of the DNA in the high viscosity buffer was measured by turning off flow and fitting the position of the distal QD (QD number 5) to an exponential decay (24). A relaxation time of $\tau_0 = 3$ s

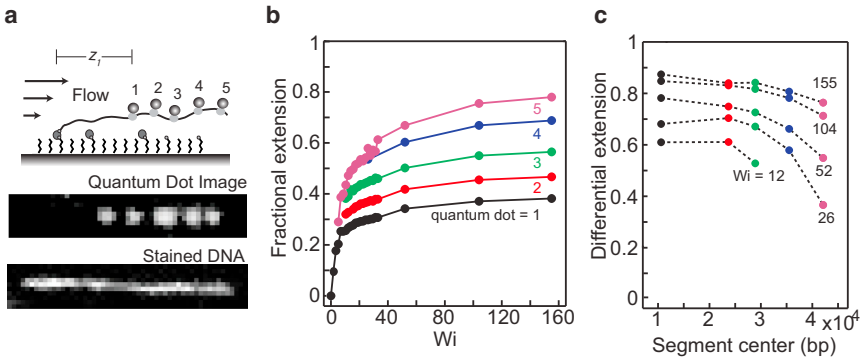

FIGURE 1 Utilization of DNA motion-capture assay to visualize flow-stretched DNAs. (*a*) Schematic of the DNA motion capture assay. Lowest image is of tethered DNA stained with SYTOX orange. (*b*) Fractional extension of labeled sites in shear flow. The QD numbering scheme is the same as in (*a*). Data for Wi $<$ 40 were taken from a single DNA in low-viscosity buffer (η = 1 cP). Data for Wi $>$ 40 were taken from a separate DNA in high-viscosity buffer (η = 15 cP). (*c*) Differential extension of shear-stretched DNAs. Note that for Wi = 12, QDs 4 and 5 could not be resolved due to overlap.

was obtained. Thus, the Wi was determined for each flow by calculating the rate of shear at the flow-cell surface using volume flow rate and flow-channel geometry. The relaxation time of the DNA in our low-viscosity buffer (1 cP) was too short to be measured due to the response time of our flow path and syringe pump. Assuming that the relaxation time scales with the viscosity, we estimated that $\tau_0 = 0.2$ s in this buffer. Extension data from DNAs taken at an equivalent Wi but different viscosity agreed (see Wi = 40 in Fig. 1 *b*), confirming our estimate.

We first measured the time-averaged conformation of the DNA for increasing Wi. Previous data collected by means of end labeling or staining with intercalating dyes have shown only the total end-to-end extension of the DNA (although intercalating dyes do give some information on internal conformation as the intensity is proportional to the areal density of DNA) (26). These data typically are expressed in the form of a fractional extension, which is the ratio of the end-to-end distance to the contour length of the DNA. At full extension, the fractional extension is equal to 1. To compare our data to published data, we define the fractional extension for each labeled site to be $\langle z_i \rangle / L$, where z_i is the distance of QD i from the tether point (i runs from 1 to 5, with $i = 1$ nearest the tether point), $\langle z_i \rangle$ is the average of this distance, and L is the contour length of the DNA (16.2 μm for λ DNA). We show our fractional extension data from two DNAs in Fig. 1 *b*. The data for Wi $<$ 40 are taken from a DNA in the low-viscosity buffer (1 cP), and the data for Wi $>$ 40 are from a DNA in the high-viscosity buffer (15 cP). These data indicate that the extension of the DNA closer to the tether point saturates at a lower Wi than the DNA near the free end. The fractional extension of QD 5, which is 3 kilobasepairs from the free end, agrees well with previously published work that measured end-to-end DNA length with an intercalating dye (see Fig. 3 *a* of Doyle et al. (23)). This agreement indicates that the hydrodynamic drag on the DNA, and not the QDs, is the major determinant of the DNA conformation.

As an additional demonstration that the fluid drag on the QDs is not significant, we measured the hydrodynamic radius of the antibody-conjugated QD using dynamic light scattering (for methods, see the Supporting Material). We find an average radius of 13.7 nm with a standard deviation of 0.4 nm. Using the Stokes-Einstein relation, we calculate a drag coefficient of approximately 2.7×10^{-10} N·s/m for each QD. This is only 3% of the longitudinal drag coefficient of λ DNA, previously reported to be 7.6×10^{-9} N·s/m (27). If we estimate the net drag on all five QDs, this is still six times smaller than the fluid drag force on the DNA.

To further elucidate how the extension at different points along the DNA varies, we parametrized the DNA contour with a variable s such that $s = 0$ at the tether point and $s = L$, the full contour length, at the free end. The location of the ith site along the contour, s_i, is then just $s_i = L \times N_i/N_{\text{total}}$, where N_i is the sequence position of the ith *Eco*RI site as measured from the tether point, and $N_{\text{total}} = 48{,}502$ for λ DNA. If we let z_i be the distance of QD i from the tether point, we can then define the differential extension of the DNA between sites $i-1$ and i as

$$\xi_i = \langle z_i - z_{i-1} \rangle / (s_i - s_{i-1}),$$

where i again runs from 1 to 5. In this equation, we define the tether point as $z_0 = s_0 = 0$. Note that this definition is a discrete approximation to the derivative of the fractional extension as a function of contour length position, s.

In Fig. 1 *c*, we show the measured differential extension for five different Wis (taken from the data shown in Fig. 1 *b*). The data are plotted versus the basepair number of the midpoint between the relevant sites, because the differential extension is an approximation to a derivative and therefore best approximates the value at the midpoint. For example, the first QD is at basepair 21,226, and we plot the differential extension for the first region (between the tether point and site 1) at half that value, or 10,613. Our data show that the differential extension is relatively constant over much of the DNA but decreases rapidly near the free end. For the Wis studied here, increasing the Wi results in a modest increase of the differential extension near

the tether point but a much larger increase at the free end. This is the differential expression of what is observed in the fractional extension (Fig. 1 *b*). As Wi increases, the plateau region (where the extension is relatively constant) extends to a larger region of the DNA as the end of the DNA unfurls in the flow.

Dynamic and static correlations in surface-tethered DNA

Site-specific labeling allows us to measure the internal dynamics of the fluctuating DNA. One striking feature of the dynamics we observed is the highly correlated motion of the QDs (see Fig. 2 *a*). To quantify these correlations, we computed the standard Pearson correlation coefficients, ρ_{ij}, from the measured trajectories.

$$\rho_{ij} = \frac{\langle \delta z_i \delta z_j \rangle}{\sqrt{\langle (\delta z_i)^2 \rangle \langle (\delta z_j)^2 \rangle}}. \quad (1)$$

In the above, the angular brackets denote a time average, and δz_i is the fluctuation in the flow direction coordinate of the ith bead away from that average, $\delta z_i = z_i - \langle z_i \rangle$. We found that the motion at all positions is highly correlated at all rates of shear measured. The motion becomes less correlated as the distance between the dots increases; for example, in the longitudinal direction correlation, coefficients vary from 0.75 (for QDs 1 and 5) to 0.98 (for adjacent QDs). As a further check, we also excluded the possibility that these strong correlations were caused by large-scale fluctuations in the flow by calculating correlation coefficients of QD trajectories from neighboring DNAs. No correlation was found within experimental uncertainties.

To determine the timescales of these correlated fluctuations, we determine the time-correlation functions of the fluctuations of the DNA at the locations of our specific labels. We define a Cartesian coordinate system such that the direction of flow is along the positive z axis and the direction of shear is along the positive x axis. Our experiments allow us to measure the z and y coordinates of the QD positions, but not the x coordinate. We then define a longitudinal correlation matrix, $C^z(\tau)$, whose matrix elements are the time-correlation functions

$$C^z_{ij}(\tau) = \langle \delta z_i(t) \delta z_j(t+\tau) \rangle, \quad (2)$$

where τ is the delay time. Note that the zero time value of this function gives the covariance in the positions of dots i and j, which appears in the numerator of Eq. 1. A similar definition holds for the transverse correlation matrix, C^y.

In principle, we should consider a total correlation matrix whose block form has C^z and C^y on the diagonal and whose off-diagonal blocks contain matrix elements of the type $\langle \delta z_i(t) \delta y_j(t+\tau) \rangle$, but these off-diagonal correlation functions were found to be zero within experimental uncertainty. Note that this is what is expected for a linear system, where the shear flow only couples motion in the direction of shear gradient to motion in the direction of flow, suggesting that a linear model might be a suitable approximation for this system.

Although the full time dependence of the autocorrelation functions is not used in our theory (developed in the next section), we show these data to demonstrate the novel measurements possible using our experimental technique. Examples of the longitudinal autocorrelation functions, the diagonal matrix elements of $C^z(\tau)$, are plotted in Fig. 2 *b* with their zero time delay values normalized to unity for a single rate of shear. The uniform decay widths of these normalized functions indicate that the timescale of relaxation for flow-direction fluctuations is roughly constant along the length of the polymer. Similar behavior is observed for the normalized transverse autocorrelation functions, as shown in Fig. 2 *c*. The highly correlated nature of the fluctuations and the single timescale that characterizes them are consistent with what would be expected according to a normal-mode picture with a dominant lowest-frequency mode. This is similar to what

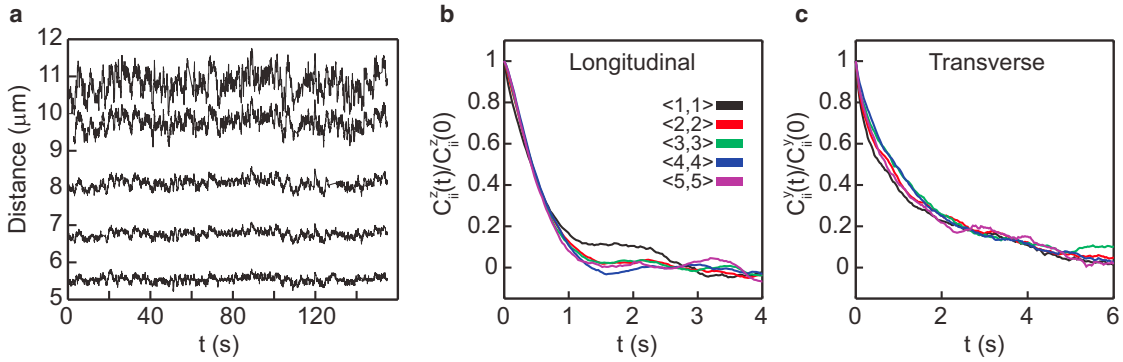

FIGURE 2 Autocorrelation functions of DNA fluctuations at Wi = 104. (*a*) Longitudinal position fluctuations of the five quantum dots along a single DNA. (*b*) Normalized autocorrelation functions for fluctuations in the flow direction. $\langle i,i \rangle$ indicates the normalized autocorrelation function $C^z_{ii}(t)/C^z_{ii}(0)$, where $C^z_{ii}(t)$ is defined with Eq. 2. See Fig. 1 *a* for QD numbering scheme. (*c*) Normalized autocorrelation functions, $C^y_{ii}(t)/C^y_{ii}(0)$, for fluctuations in the transverse direction. Labeling and color coding of data is the same as in (*b*).

has been observed for transverse fluctuations of doubly tethered DNAs under zero-flow conditions (28). We note that site-specific labeling allows us to observe this in both the transverse and the longitudinal (with the flow) direction. Futhermore, the decay rates of the autocorrelation functions increase with increasing Wi (data not shown), which is consistent with previous observations for Wi > 1 (23).

The longitudinal and transverse cross-correlation functions, the off-diagonal elements of the matrices $C^z(\tau)$ and $C^y(\tau)$, were also examined. These functions quantify the correlation between fluctuations at one point in the DNA with another point separated spatially at a later time. Examples of these cross correlation functions are shown in Fig. 3, *a* and *b*. The cross-correlation functions decay at large time with the same timescale as the autocorrelation but show a decrease at zero time delay due to the less-than-perfect correlations of the motions at the same time in different points on the DNA. A notable feature evident in the transverse cross-correlation functions is the asymmetric peak located at positive delay time. The location of this peak shifts to larger delay time as the distance between the two points increases. This is simply a consequence of the finite transmission time of deformation along the DNA chain. These peak shifts should in principle be present in the longitudinal cross-correlation functions as well, but the higher longitudinal tension due to the flow likely makes this propagation timescale very short. A small shift can be observed in the longitudinal cross-correlation function between dots 1 and 5, but the shift is too small to reliably separate from the noise in the data.

Mesoscale elastic forces in DNA

Knowledge of the extension and fluctuations of site-specific loci allows us to determine tension as a function of position

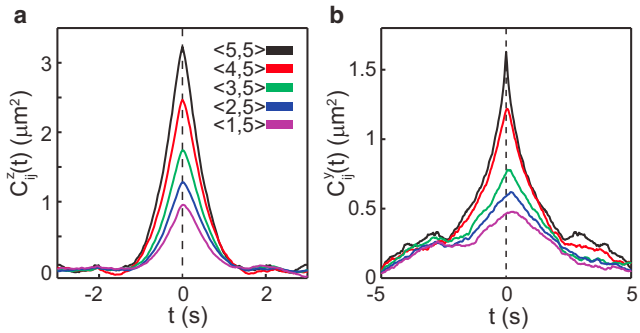

FIGURE 3 Cross-correlation functions of DNA fluctuations at Wi = 104. (*a*) Time cross-correlation functions for fluctuations in the flow direction. $\langle i,j\rangle$ indicates the cross-correlation function $C^z_{ij}(t)$ defined in Eq. 2. Correlation functions $\langle 2,5\rangle$ and $\langle 1,5\rangle$ show a slight asymmetry with respect to time. (*b*) Time cross-correlation functions, $C^y_{ij}(t)$, for fluctuations in the transverse direction. The function $C^y_{ij}(t)$ is defined as in Eq. 2. Color coding is the same as in (*a*). Note that the asymmetry in time is more pronounced in these correlation functions.

along the DNA in a model-independent way. To extract the effective interactions between the different sites on the DNA, we approximated the polymer as a bead-spring chain (34) consisting of n beads located at positions $\mathbf{r}_1$ to $\mathbf{r}_n$ relative to the origin. Each bead corresponds to one of the QD-labeled sites of the DNA, and the spring connecting two adjacent beads represents a coarse-graining of the polymer segment between those sites. The springs obey a general potential, $V_i = V_i(R_i)$, where $R_i \equiv |\mathbf{r}_i - \mathbf{r}_{i-1}|$ is the extension of the ith spring, and the index i runs from 1 to n. Different springs do not in general obey the same potential.

The DNA molecule attains mechanical equilibrium by balancing the repulsive force of the substrate against the shear-flow gradient and its intersite elastic forces (Fig. 1 *a*). The labeled dots are sufficiently far from the tether point so that they lie along a line parallel to the substrate in the flow direction. At steady state, there are no external forces acting in the y direction, so the mean displacements in this direction are zero. The mean displacements along the direction of flow, however, are manifestly nonzero. We choose the origin of the system so that the labeled sites all lie along the z axis.

We first consider the steady-state dynamics, in which the polymer fluctuates about the configuration established by mechanical equilibrium. These dynamics do not depend on the complex unfurling mechanism (35). We can define the dynamic vector extension of each labeled segment as

$$\mathbf{R}_i(t) = \overline{\mathbf{R}}_i + \delta\mathbf{R}_i(t),$$

where $\overline{\mathbf{R}}_i$ is the average vector extension of the segment, and $\delta\mathbf{R}_i(t)$ is a fluctuation in extension away from that average.

These fluctuations in extension are small, so a Taylor expansion of the potential V_i about the steady-state configuration yields

$$V_i(R_i) \approx V(\overline{R}_i) + f_i\delta Z_i + \frac{1}{2}k_{\perp,i}\left((\delta X_i)^2 + (\delta Y_i)^2\right) + \frac{1}{2}k_{\parallel,i}(\delta Z_i)^2, \tag{3}$$

where $f_i = (\partial V_i/\partial R_i)\big|_{R_i=\overline{R}_i}$ is the magnitude of the restoring force in segment i at mechanical equilibrium and δX_i, δY_i, and δZ_i are the components of the vector fluctuation, $\delta\mathbf{R}_i$. The transverse and longitudinal force constants are defined as

$$k_{\perp,i}(\overline{R}_i) = \frac{f_i}{\overline{R}_i} \text{ and } k_{\parallel,i}(\overline{R}_i) = \frac{\partial f_i}{\partial R_i}\Big|_{R_i=\overline{R}_i}, \tag{4}$$

respectively. In other words, f_i is the tension in polymer segment i at mechanical equilibrium, and $k_{\perp,i}(\overline{R}_i)$ and $k_{\parallel,i}(\overline{R}_i)$ are the linear force constants describing small harmonic motions about that equilibrium in the transverse and longitudinal directions, respectively. The above force

constants are identical in form to those derived by Hatfield and Quake (29).

In general, the motion along the y direction will be nontrivially coupled to that of the other two Cartesian directions, but these couplings are to leading order $\mathcal{O}(\delta R_i^3)$ in the Taylor expansion of the intersite potential. We are thus free, in the small fluctuation limit, to treat the transverse, out-of-flow steady-state motion independently of the motion in the other two directions using a linear Langevin equation of the form

$$\Gamma\dot{\mathbf{y}}(t) = -\mathrm{K}_\perp\mathbf{y}(t) + \boldsymbol{\zeta}(t). \tag{5}$$

In Eq. 5, $\mathbf{y}$ is a vector whose ith component is y_i, $\boldsymbol{\zeta}(t)$ is a vector whose ith component is a gaussian random force acting in the y direction on the ith labeled site, Γ is a damping constant, and $\mathrm{K}_\perp$ is a linear force constant matrix. Because we only consider the elastic interactions between adjacent beads, this force-constant matrix is sparse, with $(K_\perp)_{ij} = 0$ for $|i-j|>1$. In fact, the form of this matrix will be equivalent to that of a one-dimensional chain of beads and harmonic springs that is tethered at one end but free at the other. The values of the force constants, $k_{\perp,i}$, that populate this matrix will be flow-dependent, since for each flow the linear response will be measured about a different steady-state.

Because the steady-state fluctuations of our system are small (see the Supporting Material for more details), the random force of our Langevin equation must obey the fluctuation-dissipation theorem, and consequently, we may treat the system as if it were in thermal equilibrium. By expressing the transverse covariance matrix in terms of a canonical partition function, the relation

$$C^y(0) = k_\mathrm{B}TK_\perp^{-1} \tag{6}$$

can be derived. Equation 6 will allow us to determine values for the force constants from the experimental covariance data, which can in turn be related to the tension, f_i.

Application of theory to simulation

To test the robustness of our approximations, we applied our theory to a simulated model polymer with known, nonlinear intersite elastic forces. This model polymer was comprised of 100 beads connected in a chain by equivalent springs obeying either the finitely extensible nonlinear elastic (FENE) force law or the WLC interpolation formula of Marko and Siggia (4).

$$F_{\mathrm{FENE}}(\xi_i) = \frac{\kappa R_0\xi_i}{1-\xi_i^2} \tag{7}$$

$$F_{WLC}(\xi_i) = \kappa\left(\xi_i - \frac{1}{4} + \frac{1}{4(1-\xi_i)^2}\right). \tag{8}$$

In the above, κ is a force constant, R_0 is the maximum spring extension, and the differential extension of the ith spring, ξ_i, is defined as R_i/R_0, where R_i is the ith spring's extension. The functions F_{FENE} and F_{WLC} give the tension in the ith spring as a function of differential extension for the FENE and WLC force laws, respectively. We chose a chain consisting of 100 beads to ensure that our simulated polymer had a high dynamic range that sampled a broad region of the force curve.

In each simulation, the first bead of the chain was tethered to a surface. This surface interacted with each other bead through the repulsive part of a 9-3 Lennard-Jones potential with effective range σ and strength ϵ, both of which were set equal to unity. The constants κ and R_0 were set equal to $30\epsilon/\sigma^2$ and 1.5σ, respectively. To simulate shear flow, each bead was subjected to a force in the z direction equal to

$$\mathbf{F}_i = (0, 0, \dot{\gamma}x_i\epsilon/\sigma), \tag{9}$$

where x_i is the x coordinate of bead i and $\dot{\gamma}$ is the dimensionless shear gradient, which we chose to be 10. Hydrodynamic fluctuations were modeled using a Langevin thermostat with effective temperature $k_\mathrm{B}T/\epsilon = 1$ and a damping parameter, Γ, equal to $\sqrt{m\epsilon}/\sigma$ (the particle mass, m, was also set to unity). The simulations were performed using the LAMMPS computing package (http://lammps.sandia.gov) (30) with a time step of 0.002, 10^7 iterations to equilibrate, and 5×10^7 iterations to collect data. Data from 5×10^5 configurations were averaged to compute the transverse, out-of-flow covariance matrix, $C^y(0)$, as well as the average extension of each segment of the polymer.

Using Eq. 6, it can be shown that the force constant $k_{\perp,i}$ is related to the variance of the beads by

$$k_{\perp,i} = k_BT\left[C^y_{ii}(0) - C^y_{i-1,i-1}(0)\right]^{-1}, \tag{10}$$

where $i = 1, 2, \ldots, n$, n is the number of springs ($n = 99$ in our simulations) and $C^y_{00}(0)\equiv0$. These force constants can be related to the force itself using Eq. 4:

$$f_i(\xi_i) = R_0\xi_i k_{\perp,i}(\xi_i). \tag{11}$$

Using these equations, we were able to compute the force at each differential extension sampled by the simulations, and the results are shown in Fig. 4, plotted as force versus differential extension. The solid gray and black lines are the exact FENE and WLC force curves given by Eqs. 7 and 8. The correspondingly colored open circles are the extracted force values from our theory. The agreement between theory and simulation is quantitative, with an average error of <8 %, and the theory is unambiguously able to distinguish between the two qualitatively similar force laws.

Application of theory to experiment

The key assumption of our model is that for small fluctuations about the mechanical equilibrium, the intersite elastic forces in the polymer are both linear and local. Only

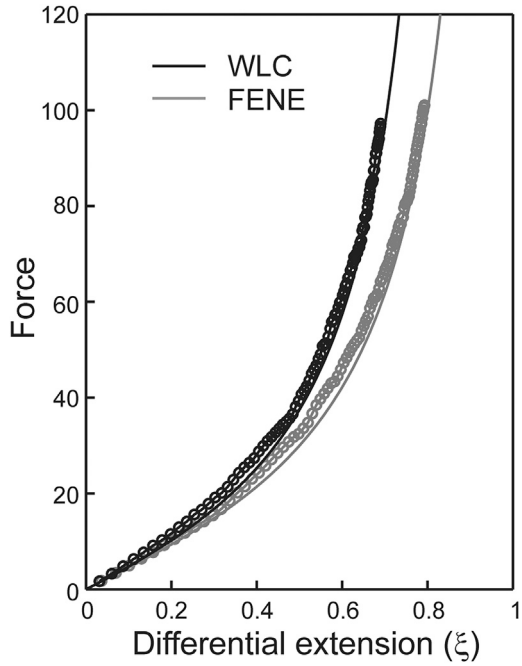

FIGURE 4 Extracted intersite force is plotted versus differential extension for the simulated FENE and WLC polymers (*gray* and *black open circles*, respectively). For both of these polymers, all segments were equivalent, so force values extracted from different segments all lie along a single curve that matches the corresponding analytic force law (*gray* and *black lines*, respectively) quantitatively.

adjacent sites along the polymer contour have a direct interaction. Since the elastic forces we characterize are merely a coarse-graining of incredibly complex electrostatic and hydrodynamic interactions that are neither linear nor local, this assumption will not hold exactly in our physical system.

The extent to which a system deviates from this assumption can be probed using the relation

$$C^{y}_{ii}(0) = C^{y}_{ij}(0), \quad j \geq i, \tag{12}$$

which is another straightforward consequence of substituting our local force matrix into Eq. 6. This relation states that for our linear and local assumption to be exact, the *y*-direction variance of each labeled site must equal its *y*-direction covariance with each site further down the chain.

If we plot the values of the matrix elements $C^{y}_{ij}(0)$ versus index j for $j \geq i$, we will generate plots of the type shown in Fig. 5. In these covariance plots, the outer boundary curve contains the points for which $i = j$, and each inner curve connects the points for which $j > i$ for each value of i. If Eq. 12 holds exactly, these inner curves will be lines of slope zero. This is very nearly the case for the simulated polymer, as shown in Fig. 5 *a* for the WLC simulation data, which is to be expected, since this system is exactly local. The DNA polymer is only approximately local, but the deviations from Eq. 12 are nonetheless small (Fig. 5 *b*).

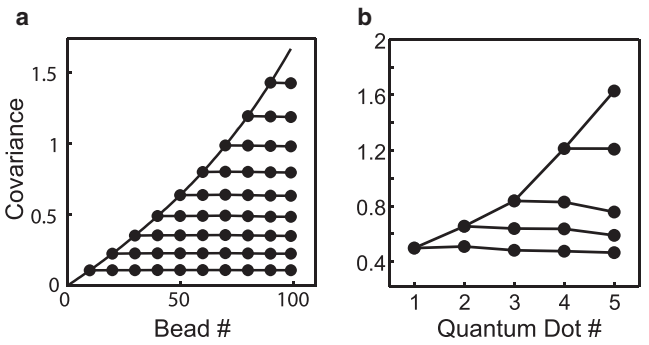

FIGURE 5 Variance and covariance plotted versus bead number for both the simulated WLC polymer (*a*) and the experimental DNA system (*b*). In both figures, the outer boundary curve plots the variance of each bead, and the inner curve connected to each point plots the covariance of that bead with each bead further down the chain. (For the simulated polymer, only every tenth bead is plotted.) For a perfectly linear and local system, the inner curves should all have slope zero. Though the experimental system has both nonlocal electrostatic and hydrodynamic forces, deviations from zero slope are still small.

The values of the tension, f_i, that we extracted from the experimental data are plotted in Fig. 6 as a function of differential extension. With the average conformation of the polymer measured in the experiments, the differential extension of each segment is easily determined from the known total contour length of λ DNA and the known base-pair positions of the *Eco*RI binding sites. Forces were extracted for segments $\langle 2,3 \rangle$, $\langle 3,4 \rangle$, and $\langle 4,5 \rangle$, the three labeled segments closest to the free end of the DNA, and the corresponding data for each segment are color-coded as red, green, and blue, respectively.

In Fig. 6, we show the results of our attempt to fit our data to the WLC interpolation force law of Marko and Siggia (4). Treating the persistence length as a free parameter, we find that on average the force-extension of these polymer

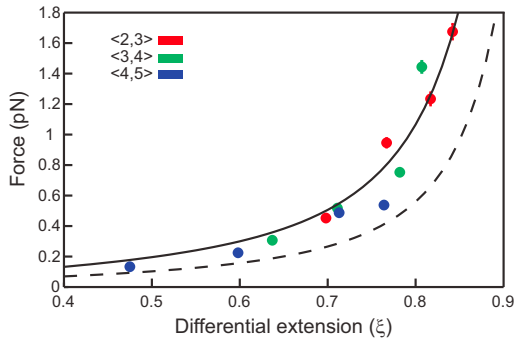

FIGURE 6 Extracted intersite force versus differential extension for the three labeled DNA segments closest to the free end. Error bars represent one standard deviation, computed by jackknifing the experimental covariance data. The extracted forces are plotted alongside the WLC force law with persistence length 26.2 nm, chosen to best fit the data (*solid line*), as well as the WLC force law with the standard DNA persistence length of 50 nm (*dashed line*).

segments is best fit by a WLC force law with an anomalous persistence length of 26 ± 6 nm (Fig. 6, *solid line*, 95% confidence interval), almost half the experimentally measured value for DNA. For comparison, the WLC force law with a persistence length of 50 nm is also plotted (Fig. 6, *dashed line*). Although experimental and theoretical studies of short DNA polymers have also extracted anomalously small persistence lengths (15,31–33), the reduction observed in these studies, if extrapolated to comparably long DNAs, was not nearly as severe.

To determine whether the anomalous persistence length we measured was due to our buffer conditions, we performed tethered-particle-motion experiments under zero-flow conditions using DNAs end-labeled with a single QD. Tethered particle motion has been used by others to measure the persistence length of DNAs (33). Previously, we have used the technique to measure the persistence length of λ DNAs end-labeled with a bead (diameter 1 μm) (39). A detailed description of the experimental methods can be found in the Supporting Material. We measured two DNAs in our low-viscosity buffer and two in the high-viscosity buffer. Measured persistence lengths varied from 65 nm to 67 nm and did not show any dependence on viscosity. These results are relatively close to the generally accepted value of 50 nm and significantly different from the anomalous value we measured for the internal segments of the DNA under shear-flow conditions.

DISCUSSION

Observing how DNA segments interact along the same strand requires tracking the motions within an individual molecule. By utilizing site-specific fluorescent probes, DNA motion capture allows us to follow the fluctuations of specific loci and thus explore DNA dynamics on the mesoscale. Whereas previous experiments using QD end-labeling of DNA have measured the end-to-end fluctuations over the entire length of the shear stretched DNA (36), our experiments provide, to our knowledge, the first characterization of both the transverse and longitudinal fluctuations throughout the DNA chain. We find that the fluctuations are highly correlated in both the transverse and longitudinal directions. Auto- and cross-correlation functions describe the timescales over which this correlation dissipates. A better understanding of the underlying motion of a flow-stretched DNA substrate can lead to improved interpretation of single-molecule experiments that probe the mechanisms of protein-DNA interactions. One application of our technique would be differentiating intrinisic DNA motion from the motion of bound proteins in the study of protein translocation along DNA (37).

Extraction of mechanical properties from the DNA motion-capture data requires a theoretical framework. In our model, we adopt a view of DNA that is coarse-grained on scales much larger than a covalent bond but small relative to the contour length of the molecule. By requiring that the model be local and linear, we are led to a generalized bead-spring model of the polymer whose parameters can be deduced directly from the experimental covariance matrix. It is interesting to note that Ladoux and Doyle (25) have shown that to understand large deformations of DNA in shear flow, both the nonlinear force-extension and the transverse fluctuations must be correctly taken into account. We have shown that information on the nonlinear force-extension behavior of mesoscopic subsegments of the DNA is contained in the covariance matrix of the transverse fluctuations.

The elastic forces we extracted for several segments along the DNA backbone were well fit, on average, by a standard WLC force law with a persistence length of 26 ± 6 nm, smaller than the accepted value of 50 nm. The persistence length we measured for the internal segments of the DNA was also significantly different from that measured for the entire DNA under zero-flow conditions in our buffers (65–67 nm). The persistence length of DNA is not an intrinsic property of DNA; for example, it can be as low as 39 nm in certain buffers (31). In addition, it is normally determined by fitting experimental data to a model that assumes specific boundary conditions for the polymer. For a long polymer, the boundary conditions will not significantly impact the bulk mechanical properties, but for shorter polymers, Seol et al. (15) found that less restrictive boundary conditions on the orientation of the polymer at its attachment points resulted in less extensibility for a given applied force. This resulted in fitted persistence lengths as low as 42 nm for short DNAs (0.6 μm). A recent tethered-particle-motion study of 1.6 μm DNAs (comparable to the 2 μm length of the intra-strand segments observed in our experiments) determined a mean persistence length of 35 nm for these DNAs (33). For a polymer segment that is part of a longer molecule, as in our case, the boundary conditions are even less restrictive, since the position, as well as the orientation, of its endpoints can vary. We would thus expect such a polymer segment to exhibit even stiffer force-extension behavior than a polymer molecule of the same length, consistent with the significantly shorter persistence length we observe in our WLC fitting.

By measuring mesoscale forces in a single DNA molecule, we present a picture of DNA mechanics that is more complex, and richer, than those given by earlier studies. The motion-capture method has immediate applications in the elucidation of how DNA binding proteins, which interact with their substrates on the basepair length scale, influence DNA structure on mesoscopic length scales (38).

SUPPORTING MATERIAL

Supporting Materials and Methods, two figures, and two tables are available at http://www.biophysj.org/biophysj/supplemental/S0006-3495(15)00402-6.

AUTHOR CONTRIBUTIONS

J.J.L., A.C.P., K.R.P., and J.D.E. designed the research. A.C.P., T.G.W.G., D.S., and K.R.P. performed the research. A.C.P., D.S., and K.R.P. analyzed the data. J.J.L., A.C.P., K.R.P., and J.D.E. wrote the article.

ACKNOWLEDGMENTS

We thank Carla Estridge for initial efforts in the molecular dynamics simulations.

J.D.E. thanks the University of Colorado for startup funds. Support for this work also comes from National Science Foundation CAREER Award MCB-1148818 (to J.J.L.) and National Science Foundation RUI Award PHYS-1205814 (to A.C.P.).

REFERENCES

1. Yu, G., A. Kushwaha, …, Z. Bao. 2011. The shear flow processing of controlled DNA tethering and stretching for organic molecular electronics. *ACS Nano.* 5:275–282.
2. Yan, H., X. Zhang, …, N. C. Seeman. 2002. A robust DNA mechanical device controlled by hybridization topology. *Nature.* 415:62–65.
3. Bustamante, C., W. Cheng, and Y. X. Mejia. 2011. Revisiting the central dogma one molecule at a time. *Cell.* 144:480–497.
4. Marko, J. F., and E. D. Siggia. 1995. Stretching DNA. *Macromolecules.* 28:8759–8770.
5. Aragón, S. R., and R. Pecora. 1985. Dynamics of wormlike chains. *Macromolecules.* 18:1868–1875.
6. Bustamante, C., J. F. Marko, …, S. Smith. 1994. Entropic elasticity of λ-phage DNA. *Science.* 265:1599–1600.
7. Kindt, J., S. Tzlil, …, W. M. Gelbart. 2001. DNA packaging and ejection forces in bacteriophage. *Proc. Natl. Acad. Sci. USA.* 98:13671–13674.
8. Yan, J., and J. F. Marko. 2003. Effects of DNA-distorting proteins on DNA elastic response. *Phys. Rev. E Stat. Nonlin. Soft Matter Phys.* 68:011905.
9. van Noort, J., S. Verbrugge, …, R. T. Dame. 2004. Dual architectural roles of HU: formation of flexible hinges and rigid filaments. *Proc. Natl. Acad. Sci. USA.* 101:6969–6974.
10. Bustamante, C., S. B. Smith, …, D. Smith. 2000. Single-molecule studies of DNA mechanics. *Curr. Opin. Struct. Biol.* 10:279–285.
11. Bustamante, C., Z. Bryant, and S. B. Smith. 2003. Ten years of tension: single-molecule DNA mechanics. *Nature.* 421:423–427.
12. Rouse, Jr., P. E. 1953. A theory of the linear viscoelastic properties of dilute solutions of coiling polymers. *J. Chem. Phys.* 21:1272–1280.
13. Marciano, Y., and F. Brochard-Wyart. 1995. Normal modes of stretched polymer chains. *Macromolecules.* 28:985–990.
14. Zimm, B. H., and J. K. Bragg. 1959. Theory of the phase transition between helix and random coil in polypeptide chains. *J. Chem. Phys.* 31:526–535.
15. Seol, Y., J. Li, …, M. D. Betterton. 2007. Elasticity of short DNA molecules: theory and experiment for contour lengths of 0.6–7 μm. *Biophys. J.* 93:4360–4373.
16. Vafabakhsh, R., and T. Ha. 2012. Extreme bendability of DNA less than 100 base pairs long revealed by single-molecule cyclization. *Science.* 337:1097–1101.
17. Wiggins, P. A., T. van der Heijden, …, P. C. Nelson. 2006. High flexibility of DNA on short length scales probed by atomic force microscopy. *Nat. Nanotechnol.* 1:137–141.
18. Cohen, A. E., and W. E. Moerner. 2007. Principal-components analysis of shape fluctuations of single DNA molecules. *Proc. Natl. Acad. Sci. USA.* 104:12622–12627.
19. King, K., S. J. Benkovic, and P. Modrich. 1989. Glu-111 is required for activation of the DNA cleavage center of EcoRI endonuclease. *J. Biol. Chem.* 264:11807–11815.
20. Finkelstein, I. J., M.-L. Visnapuu, and E. C. Greene. 2010. Single-molecule imaging reveals mechanisms of protein disruption by a DNA translocase. *Nature.* 468:983–987.
21. Reference deleted in proof.
22. Thompson, R. E., D. R. Larson, and W. W. Webb. 2002. Precise nanometer localization analysis for individual fluorescent probes. *Biophys. J.* 82:2775–2783.
23. Doyle, P. S., B. Ladoux, and J. L. Viovy. 2000. Dynamics of a tethered polymer in shear flow. *Phys. Rev. Lett.* 84:4769–4772.
24. Lueth, C. A., and E. S. G. Shaqfeh. 2009. Experimental and numerical studies of tethered DNA shear dynamics in the flow-gradient plane. *Macromolecules.* 42:9170–9182.
25. Ladoux, B., and P. S. Doyle. 2000. Stretching tethered DNA chains in shear flow. *Europhys. Lett.* 52:511–517.
26. Perkins, T. T., D. E. Smith, …, S. Chu. 1995. Stretching of a single tethered polymer in a uniform flow. *Science.* 268:83–87.
27. Meiners, J.-C., and S. R. Quake. 2000. Femtonewton force spectroscopy of single extended DNA molecules. *Phys. Rev. Lett.* 84:5014–5017.
28. Crut, A., D. Lasne, …, P. Desbiolles. 2003. Transverse fluctuations of single DNA molecules attached at both extremities to a surface. *Phys. Rev. E Stat. Nonlin. Soft Matter Phys.* 67:051910.
29. Hatfield, J. W., and S. R. Quake. 1999. Dynamic properties of an extended polymer in solution. *Phys. Rev. Lett.* 82:3548–3551.
30. Plimpton, S. 1995. Fast parallel algorithms for short-range molecular dynamics. *J. Comput. Phys.* 117:1–19.
31. Wang, M. D., H. Yin, …, S. M. Block. 1997. Stretching DNA with optical tweezers. *Biophys. J.* 72:1335–1346.
32. Knotts, 4th, T. A., N. Rathore, …, J. J. de Pablo. 2007. A coarse grain model for DNA. *J. Chem. Phys.* 126:084901.
33. Brinkers, S., H. R. C. Dietrich, …, B. Rieger. 2009. The persistence length of double stranded DNA determined using dark field tethered particle motion. *J. Chem. Phys.* 130:215105.
34. Underhill, P. T., and P. S. Doyle. 2004. On the coarse-graining of polymers into bead-spring chains. *J. Nonnewton Fluid Mech.* 122:3–31.
35. Hallatschek, O., E. Frey, and K. Kroy. 2005. Propagation and relaxation of tension in stiff polymers. *Phys. Rev. Lett.* 94:077804.
36. Laube, K., K. Günther, and M. Mertig. 2011. Analysis of the fluctuations of a single-tethered, quantum-dot labeled DNA molecule in shear flow. *J. Phys. Condens. Matter.* 23:184119.
37. Tafvizi, A., F. Huang, …, A. M. van Oijen. 2011. A single-molecule characterization of p53 search on DNA. *Proc. Natl. Acad. Sci. USA.* 108:563–568.
38. Graham, T. G. W., X. Wang, …, J. J. Loparo. 2014. ParB spreading requires DNA bridging. *Genes Dev.* 28:1228–1238.
39. Song, D., B. Mousley, …, A. C. Price. 2015. Tethered particle motion with single DNA molecules. *Am. J. Phys.* 83:418.